

Influence of hydrogen radicals treatment on layers and solar cells made of solution-processed amorphous silicon

Torsten Bronger,¹ Jan Wördenweber,¹ Paul Wöbkenberg,² Stefan Muthmann,¹ Odo Wunnicke,² and Reinhard Carius¹

¹*Forschungszentrum Jülich GmbH, Institut für Energie und Klimaforschung (IEK-5), Jülich, 52425 (Germany)*

²*Evonik Industries AG Paul-Baumann Str. 1, Marl, 45772 (Germany)*

Solution-processed amorphous silicon is a promising material for semiconductor devices. Unfortunately, its manufacturing leaves a high density of defects in the layer, which can be reduced by a treatment with hydrogen radicals. Here, we present an optimized hydrogen treatment, which is used for best performing solar cells made of solution-processed amorphous silicon. We examine the amount and the nature of hydrogen incorporation using infrared absorption and hydrogen effusion. The hydrogen treatment not only increases hydrogen content significantly, it also enlarges the fraction of hydrogen in a bonding configuration which is known to be advantageous for electronic properties, albeit only close to the surface. Using electron spin resonance and photothermal deflection spectroscopy spectra, we confirm a reduction of defect density. Regarding the electrical properties, the ratio of photo and dark conductivity is increased by almost two decades. This leads to a greatly enhanced performance of solar cell devices which use the material as the absorber layer. In particular, the efficiency jumps by a factor of three.

Since the work of Shimoda[1], solution-processed amorphous silicon made of cyclopentasilane (CPS) and neopentasilane (NPS) precursors has gained interest for the application in semiconductor devices, in particular solar cells. Recently, solar cells based on this material reached an efficiency of 3.5% [2]. However, immediately after the conversion of the polymer into a silicon layer, layer quality is poor.[4] Thus, a treatment with hydrogen radicals is applied to bring hydrogen back into the layer.[2, 4, 5] Since this is a crucial step in the processing, it is worth having a close look at it.

For details of layer and stack preparation, including the doping of the material, see the experimental section in Ref. 2.

For the hydrogen radicals treatment, the sample is mounted on a holder in a vacuum chamber (approx. $4 \cdot 10^{-7}$ mbar). It is tempered for one hour at 370°C, so that the heat is homogeneously distributed and the surface water film evaporated. Then, 30 sccm of hydrogen gas (chamber pressure is then at 0.1 mbar) pass the layer. At the same time, a tantalum filament at 1350°C with a distance of 6.8 mm to the sample decomposes the hydrogen. The sample is heated with the same power as in the tempering step, however the filament would have an additional thermal impact, which we have not measured. This passivation step takes 2 hours, after which the sample is thermalized to room temperature and transferred out of the chamber into ambient atmosphere.

A dip of the sample in hydrofluoric acid (10%) ca. 3 minutes before the transfer into vacuum does not improve layer or cell performance. However, it is very important to check the chamber wall for deposits. We observed black discoloration on the wall after a couple of hydrogen treatment runs, which negatively affected passivation effectiveness.

The Raman spectra are measured with an excitation wavelength of 488 nm. Our in-house design is capable of a resolution of 0.5 cm^{-1} . Moreover, we used a widened laser spot of $50 \times 1 \mu\text{m}$ in size in order to be able to

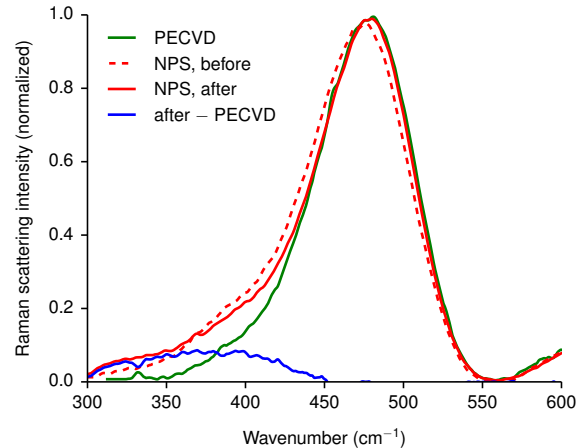


FIG. 1. Spectrum of Raman scattering of intrinsic NPS and state-of-the-art PECVD material. The amorphous silicon peaks are normalized to 1.

average over layer inhomogeneities.

Fig. 1 shows the Raman scattering spectrum of intrinsic layers fabricated of NPS. The dominating peak is that of amorphous silicon with no measurable crystalline volume fraction. In contrast to PECVD material, the peak is slightly shifted towards smaller wavenumbers, and broadened. Tab. I quantifies these differences. These two deviations from the PECVD reference spectrum are largely compensated by the treatment with hydrogen radicals, as visualized in Fig. 1 and shown in Tab. I. The residual difference is plotted in blue in Fig. 1.

One may deduce from these results that the hydrogen treatment reduces the stress. This is backed by the peeling-off of very thick layers. Thus, we know that it suffers from tensile stress. However, this explanation is put in question by crack formation and propagation being independent of the hydrogen treatment. Moreover, the mechanism of stress reduction is unclear. An alternative

TABLE I. Electrical and optical properties of NPS material at room temperature. The optical gap is the energy at which the absorption coefficient equals 10^{-4} cm^{-1} , as determined by the PDS technique. Typical values for state-of-the-art PECVD material are shown for comparison.

	before	after	PECVD
	hydrogen treatment		reference
Raman peak shift (cm^{-1})	-6.8	-2.7	0
Raman peak width (cm^{-1})	75.3	72.2	70.8
optical gap (eV)	1.95	1.99	1.98
optical band tail width (meV)	86	78	61
absorption at 1.2 eV (cm^{-1})	24	7.0	4
hydrogen content (%)	6.9	8.4	17
micro structure factor (%)	64	52	22
dark conductivity (S/cm)	$2.2 \cdot 10^{-10}$	$3.3 \cdot 10^{-11}$	$1.4 \cdot 10^{-10}$
photo conductivity (S/cm)	$2.2 \cdot 10^{-7}$	$2.5 \cdot 10^{-6}$	$3.4 \cdot 10^{-5}$
photo/dark conductivity ratio	$1.0 \cdot 10^3$	$7.7 \cdot 10^4$	$2.4 \cdot 10^5$

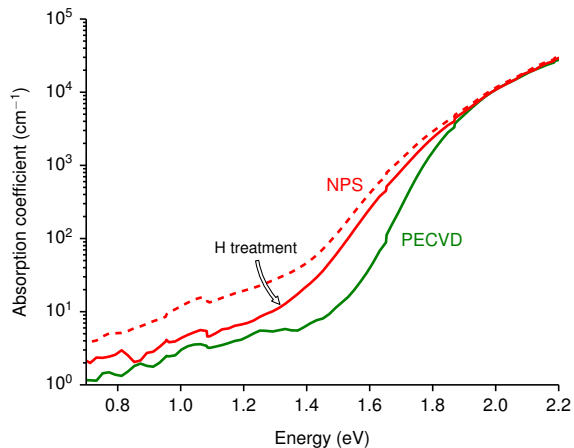


FIG. 2. The absorption coefficient versus photon energy of intrinsic layers of NPS and PECVD material as measured with the PDS technique. The thickness of the NPS sample is approximately 134 nm, while that of the PECVD sample is 200 nm.

explanation for the shift would be a peak at 460 cm^{-1} which vanishes or is strongly suppressed after the treatment, but also here, the mechanism would be unclear. Future substrate curvature measurements as an estimate for the layer tension may provide further insight.

The residual difference between hydrogen-treated NPS material and PECVD material (blue in Fig. 1) can be easily explained by an enhanced longitudinal optical (LO) phonon absorption at 380 cm^{-1} in NPS. Generally, this indicates increased disorder in the microstructure.[12]

For the absorption measurements, we use a photothermal deflection spectroscopy (PDS) in-house design. A cuvette filled with carbon tetrachloride takes the sample. Our monochromator after a hydrogen lamp allows an output bandwidth of 10 meV, however, the data points are spaced by 20 meV. The integral irradiation power on the

sample is approx. $1 \mu\text{W}$.

Fig. 2 depicts the absorption spectrum of an intrinsic NPS layer, measured with the PDS technique. NPS exhibits a strongly enhanced absorption in the critical domain below 2 eV. The optical tail width, which we define as the maximal slope of the curve in semi-logarithmic axes, is substantially higher than in the PECVD case. The same is true for the absorption at 1.2 eV. Similarly to the Raman results, the hydrogen treatment diminishes the differences between the NPS layer and the reference layer. Tab. I confirms this observation quantitatively. Additionally, it gives the value of the optical gap for all cases. Again, the hydrogen treatment brings this value closer to the PECVD reference.

The hydrogen treatment saturates the dangling bonds, thus the absorption at 1.2 eV is reduced. This is confirmed strongly by the very good correlation of PDS and ESR results (see Fig. 3). Furthermore, the decrease in tail width is interpreted as less disorder in microstructure, which matches nicely the lower LO phonon absorption in Raman scattering. This also leads to the increased optical gap as defined in Tab. I.

Conventional continuous wave electron spin resonance (ESR) measurements are performed with a commercial X-band ($\nu = 9.3 \text{ GHz}$) Bruker Elexsys E500 spectrometer in a cylindrical mode resonator at room temperature, microwave power of $4 \cdot 10^{-5} \text{ W}$, magnetic field modulation amplitude of 5 G, and modulation frequency of 100 kHz. A calibrated sputtered amorphous silicon sample with a spin density of $2 \cdot 10^{15} \text{ cm}^{-3}$ and g-value of 2.00565 was used as a reference standard.

Fig. 3 combines the results of PDS and ESR measurements. The optical absorption at 1.2 eV is proportional to the defect density as measured with ESR,[8, 9] and indeed this dependency is reproduced by NPS samples with high accuracy over 2.5 orders of magnitude. Ref. 8 reports a proportionality factor in the range $1.2\text{--}2.5 \cdot 10^{16} \text{ cm}^{-2}$, which is shaded in gray in Fig. 3. Obvi-

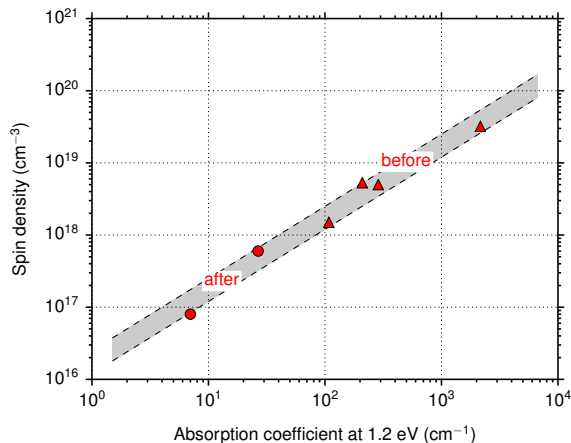


FIG. 3. Dependency of spin density on optical absorption at 1.2 eV. Samples before the hydrogen treatment (red triangles) as well as after (red discs) are included. The gray corridor is taken from Ref. 8 and bases on a comprehensive results compilation.

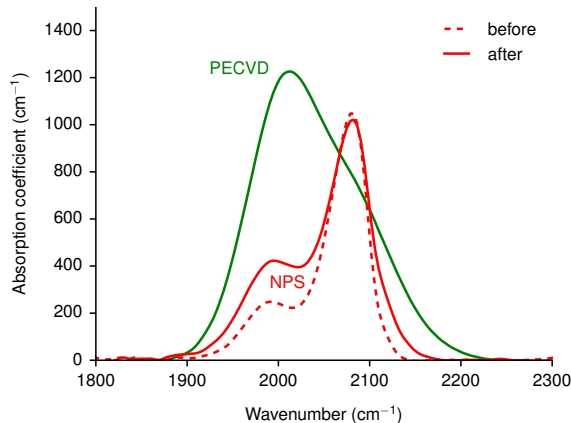


FIG. 4. Infrared absorption spectrum of intrinsic NPS (230 nm) and PECVD (700 nm) layers, deposited on silicon wafer substrate. The dashed line denotes material before the hydrogen treatment. This plot is taken from the supplementary information of Ref. 2.

ously, the NPS samples both before and after the hydrogen treatment stay in this range.

For the infrared absorption measurements, we deposited the NPS layer on double-side polished silicon wafer. The measurement data itself is collected by an FTIR spectrometer (Nicolet 5700) with a glow bar as light source. We subtracted the absorption spectrum of a piece of uncovered silicon wafer, and subtracted an additional, manually tweaked spline baseline.

Fig. 4 shows infrared absorption spectrum of an NPS layer. There are two peaks of interest here, one at approx. 2000 cm^{-1} and the other at approx. 2080 cm^{-1} . Both are identified with Si-H oscillation modes, however of hydrogen in different bonding configurations. In particular, the 2080 peak is related to bonds at (inner) surfaces,[10]

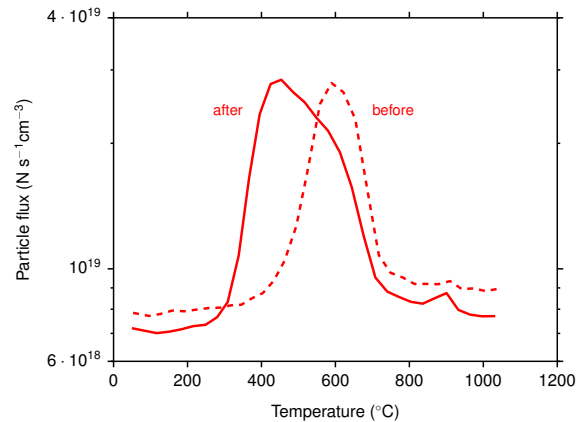


FIG. 5. Hydrogen effusion diagram of an intrinsic NPS layer before and after the hydrogen treatment.

which is not able to actually passivate dangling bonds in the bulk. In contrast, the 2000 peak is considered “good” hydrogen in the sense of decreasing bulk defect density. Quantitatively, this is expressed by the microstructure factor (MSF).[11] Generally speaking, a smaller MSF indicates a better material.

As one can see in Tab. I, in NPS layers, the MSF is significantly higher than in PECVD reference layers. One can also see that the hydrogen treatment ameliorates this situation to some extent. Fig. 4 shows that this is achieved by increasing the bulk hydrogen while leaving the hydrogen at inner surfaces constant. Accordingly, the integral hydrogen content raises by 20%. However, the content of passivating hydrogen is still much lower than in PECVD material.

These findings are accompanied by hydrogen effusion measurements that are presented in Fig. 5. Hydrogen effusion is measured in the setup described in Ref. 7, a so-called open system with a turbomolecular pump. The base pressure is approx. 10^{-10} mbar and the heating rate $20^\circ\text{C}/\text{min}$. NPS layers emit most hydrogen at 600°C . After the hydrogen treatment, there is an additional emission at 400°C . Note that absolute peak heights bear a high uncertainty in such measurements. In particular, the fact that the original peak at 600°C is still visible but slightly smaller after the hydrogen treatment need not be a real effect. However, the temperature axis is accurate enough, and the peak separation large enough, to state that the incorporated hydrogen is located and/or bonded differently from the hydrogen that was already in the material.

IR absorption and effusion measurements give complementary information about how the hydrogen is incorporated into the layer. On the one hand, IR absorption clearly shows that virtually the complete additional hydrogen is passivating dangling bonds, which certainly is an encouraging result. On the other hand, effusion suggests that this hydrogen does not reach the inner parts of the layer. Instead, it gets stuck close to the surface.

TABLE II. Solar cell properties at room temperature. Typical values for state-of-the-art PECVD material are shown for comparison.

	effective cell area in mm ²	efficiency in %	I_{sc} in mA cm ⁻²	V_{oc} in mV	fill factor in %	series resistance in Ohm
before H treatment	3.2	0.68	4.4	497	31.1	2,400
after H treatment	3.2	2.0	7.4	628	42.7	910
best NPS cell[2]	3.2	3.5	9.0	730	53.8	550
PECVD[2]	3.2	5.9	9.8	892	67.5	450

Note that “surface” includes here also inner surfaces of cracks and tunnels and structures of enhanced hydrogen diffusion.

For determining the electrical conductivity, we evaporated two silver pad contacts at a distance of 0.5 mm on the sample. Then, we heat it in vacuum at 420 K for 30 minutes in order to evaporate most of the surface water film. The measurement itself is performed at room temperature using a Keithley 617 electrometer. We measure the electrical current at voltages between -100 and $+100$ V in order to detect non-ohmic behavior. For photoconductivity measurements, a xenon halogen lamp in conjunction with an infrared filter (Schott KG 7) provides the illumination.

Tab. I includes the results of photo and dark conductivity measurements. They exhibit the most drastic change by hydrogen treatment. The dark conductivity decreases, which is advantageous for the use in some types of devices. But much more importantly, the photo conductivity and the photo/dark ratio increase, the latter by a factor of almost 100. All of these changes make the material more suitable as an absorber material in solar cells.

The defects and band tail states as discussed in the preceding paragraphs are detrimental for electronic transport under illumination. Defects are recombination centres for charge carriers,[13] and band tail states are traps for them.[14] This explains the greatly increased photoconductivity after the hydrogen treatment. For dark conductivity, however, the Fermi level moves away from the mobility edge if less deep defects are present, so that the charge carrier balance is fulfilled. This causes a lower carrier concentration in the extended states above the mobility edge, and therefore, decreases dark conductivity.

We measure characteristic IV curves using a Keithley 238 source measure unit in a sun simulator with AM1.5 spectrum (class A), with a data point spacing of 10 mV. During the measurement, we keep the sample at room temperature $\pm 1^\circ\text{C}$.

Tab. II and Fig. 6 show the influence of the hydrogen treatment on solar cell devices. Because the best cell published in Ref. 2 was not measured before passivation, we present a comparison of a less efficient production

run. Nevertheless, the best cell results are included for comparison, as are PECVD reference cell results. Note

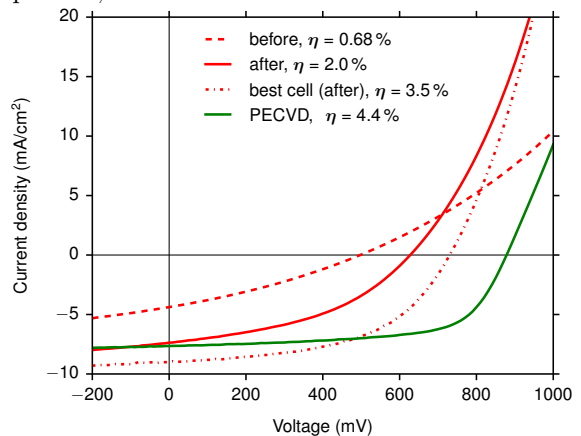


FIG. 6. Characteristic IV curve before and after the hydrogen treatment. For comparison, we included the curve of our best cell device as published in Ref. 2, and a PECVD reference.

that the latter are adapted to the smaller thickness of the NPS layers. The details of this adaption can be found in Ref. 2.

The hydrogen treatment significantly improves the cell characteristics in any respect. Most prominently, the series resistance (measured as the inverse slope at the V_{oc} point) drops by a factor of 2.6. I_{sc} , V_{oc} , and fill factor are increased by 68%, 26%, and 35% respectively, and the efficiency, which is a combination of these quantities, is tripled.

Note that the massive improvement in cell performance is attributed to the hydrogen treatment alone, and thus is orthogonal to all other conceivable optimization techniques (e.g. light trapping, thickness optimization, conversion optimization, interface improvements).

A lack of electronic and optical quality in comparison to PECVD material remains. Both the density of defects and the widths of the band tails need to be reduced to allow higher fill factor and open-circuit voltage. Moreover, only surface-near regions are passivated so far, which needs to be extended into the bulk.

-
- [1] T. Shimoda, Y. Matsuki, M. Furusawa, T. Aoki, I. Yudasaka, H. Tanaka, H. Iwasawa, D. Wang, M. Miyasaka, and Y. Takeuchi, *Nature* **440**, 783 (2006).
- [2] T. Bronger, P. H. Wöbkenberg, J. Wördenweber, S. Muthmann, U. W. Paetzold, V. Smirnov, S. Traut, Ü. Dagkaldiran, S. Wieber, M. Cölle, *et al.*, *Advanced Energy Materials* (2014).
- [3] H. Dersch, J. Stuke, and J. Beichler, *Applied Physics Letters* **38**, 456 (1981).
- [4] T. Masuda, N. Sotani, H. Hamada, Y. Matsuki, and T. Shimoda, *Applied Physics Letters* **100**, 253908 (2012).
- [5] T. Sontheimer, D. Amkreutz, K. Schulz, P. H. Wöbkenberg, C. Guenther, V. Bakumov, J. Erz, C. Mader, S. Traut, F. Ruske, *et al.*, *Advanced Materials Interfaces* **1** (2014).
- [6] O. Kluth, B. Rech, L. Houben, S. Wieder, G. Schöpe, C. Beneking, H. Wagner, A. Löffl, and H. Schock, *Thin Solid Films* **351**, 247 (1999).
- [7] W. Beyer and F. Einsele, “Hydrogen effusion experiments,” in *Advanced Characterization Techniques for Thin Film Solar Cells* (Wiley, 2011) Chap. 17.
- [8] N. Wyrsh, F. Finger, T. McMahon, and M. Vanecek, *Journal of non-crystalline solids* **137**, 347 (1991).
- [9] W. B. Jackson and N. M. Amer, *Physical Review B* **25**, 5559 (1982).
- [10] M. Cardona, *physica status solidi (b)* **118**, 463 (1983).
- [11] A. Mahan, P. Raboisson, D. Williamson, and R. Tsu, *Solar Cells* **21**, 117 (1987).
- [12] J. Gerbi, P. Voyles, M. Treacy, J. Gibson, and J. Abelson, *Applied physics letters* **82**, 3665 (2003).
- [13] B. Abeles, G. Cody, Y. Goldstein, T. Tiedje, and C. Wronski, *Thin Solid Films* **90**, 441 (1982).
- [14] T. Tiedje, *Applied Physics Letters* **40**, 627 (1982).